First Exclusive Measurement of Deep Virtual Compton Scattering off 4He: Toward the 3D tomography of nuclei

M. Hattawy,[1,2] R. Dupré,[1,2] N.A. Baltzell,[1,3] and K. Hafidi[1,*]

(The CLAS Collaboration)

[1]*Argonne National Laboratory, Argonne, Illinois 60439*
[2]*Institut de Physique Nucléaire, CNRS/IN2P3 and Université Paris Sud, Orsay, France*
[3]*Thomas Jefferson National Accelerator Facility, Newport News, Virginia 23606*
(Dated: January 22, 2017)

We report the first exclusive measurements of deeply virtual Compton scattering (DVCS) off a nucleus, where all the products of the reaction including the recoil 4He nucleus were detected. The experiment was performed using the Jefferson Lab CEBAF Large Acceptance Spectrometer (CLAS) enhanced with a radial time projection chamber (RTPC) to detect the recoiling 4He nuclei. We measure large beam spin asymmetries comparable to the proton's ones and extract in a model independent way, the single chirally-even generalized parton distribution of the 4He nucleus. These are pioneering measurements and will lead the way toward the 3D imaging of the partonic structure of nuclei.

A wealth of information on the quantum chromodynamics (QCD) structure of hadrons lies in the correlations between the momentum and spatial degrees of freedom of the fundamental constituent partons, quarks and gluons. Such correlations are accessible via the generalized parton distributions (GPDs). The GPDs correspond to the coherence between quantum states of different (or same) helicity, longitudinal momentum, and transverse position. In an impact parameter space, they can be interpreted as a distribution in the transverse plane of partons carrying a certain longitudinal momentum [1–3]. A crucial feature of GPDs is the access to the transverse position of partons which, combined with their longitudinal momentum, leads to the total angular momentum of partons [4]. Deep virtual Compton scattering (DVCS) corresponding to hard exclusive electroproduction of a real photon, which is considered as the cleanest probe to access GPDs and thus study the 3D imaging of nucleons and nuclei.

DVCS measurements have been the focus of a worldwide effort [5–15] involving several accelerator facilities such as Jefferson Lab (JLab), HERA and CERN. The vast majority of the experiments focused on the study of the nucleon's structure. The deuterium was also investigated at HERMES and JLab [16] mainly as a neutron target. However, studying the 3D imaging of the nucleon is a very important goal, understanding how these distributions are modified to provide the binding and structure in a nucleus is as fascinating of a question and an integral part of our quest of using QCD to explore nuclear matter.

A DVCS process on a nuclear target differ from single nucleon scattering in providing access to the measure two DVCS channels. In the coherent DVCS channel, the target nucleus (A) remains intact and recoils as a whole while emitting a real photon ($eA \rightarrow e'A'\gamma$), allowing to measure the nuclear GPDs of the target. In the incoherent channel, the nucleus breaks up and the DVCS takes place on a bound nucleon (N) that emits the final photon ($eA \rightarrow e'N'\gamma$ X), enabling the GPDs measurement of the bound nucleons and to study their modifications in the nuclear medium via the GPDs. Figure 1 illustrates the dominant mechanism for the coherent DVCS channel on 4He. At sufficiently large squared electron momentum transfer Q^2 ($= -(k - k')^2$) and small squared momentum transfer t ($= (p - p')^2$), the QCD factorization theorem predicts that the DVCS handbag diagram can be factorized into two parts, hard and soft parts [17, 18]. The hard part includes photons-quark interaction and it is calculable through perturbative methods, while the soft/non-perturbative part is parametrized in terms of GPDs, which embed the partonic structure of the hadron. Experimentally, the DVCS reaction is indistinguishable from the Bethe-Heitler (BH) process, which is the reaction where the final photon is emitted either from the incoming or the outgoing leptons. The BH process is not sensitive to GPDs and does not carry information about the partonic structure of the hadronic target. The BH cross section is calculable from the well-known electromagnetic form factors.

The GPDs are defined for each quark flavor and gluon as matrix elements of the light cone operators [19], describing the transition between the initial and final states of a hadron. The GPDs depend on two longitudinal momentum fraction variables (x, ξ) and on the momentum transfer t to the target. x is the average longitudinal momentum fraction of the parton involved in the process and ξ is the longitudinal fraction of the momentum
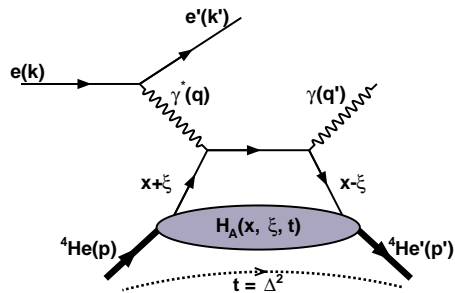
FIG. 1: Deep virtual Compton scattering process in the hand-bag approximation.
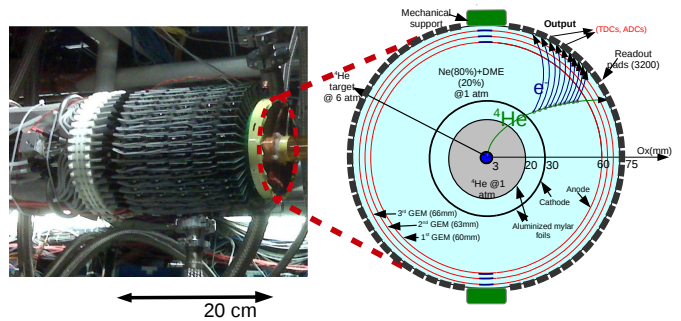

FIG. 2: Left: A picture of the CLAS-EG6 RTPC before insertion into the solenoid. Right: A cross section of the CLAS-EG6 RTPC perpendicular to the beam direction. An illustration of a ^{4}He track originating from the pressurized straw target is shown along with the electrons produced in the drift region.

transfer t, which is related to the Bjorken variable x_B: $\xi \approx \frac{x_B}{2-x_B}$, where $x_B = \frac{Q^2}{2M\nu}$ with the proton mass M and $\nu = E_e - E_{e'}$. The GPDs x variable cannot be measured experimentally in a DVCS reaction. Hence, we measure the their convolutions on x, the so-called Compton Form Factors (CFF) [20]. In a DVCS process, the number of GPDs needed to parametrize the partonic structure of a hadron depends on the different configurations between the spin of the hadron and the helicity direction of the struck quark. Therefore, the partonic structure of spin zero nuclei, such as ^4He and ^{12}C, is parametrized by only one GPD ($H_A(x, \xi, t)$) at leading twist, while 4 GPDs arise in the nucleon case. In this work, we have chose the ^{4}He nucleus as our target of interest because of it's spinless nature and it shows a clear EMC effect [21], in addition of having a high density and it is a well-known few-body system.

The study of nuclear DVCS is still in its infancy due to the challenging detection of the low-energy recoil nuclei in fixed target experiments. Until very recently, the HERMES experiment [25] was the only one to measure DVCS off heavier nuclei such as ^{4}He, N, Ne, Kr and Xe, where only the scattered electron and the real photon are detected. In this paper, we report the first exclusive measurements of the coherent DVCS channel off ^{4}He where all products of the reaction are detected including the recoiling ^{4}He nucleus. Following this exclusive measurement, the ^{4}He CFF ($\mathcal{H}_A$) will be extracted experimentally in a fully model independent way for the first time ever. The incoherent DVCS channel measurement from the same data set in in preparation and will reported in another publication.

The experiment, CLAS-EG6, took place in the experimental Hall-B of Jefferson laboratory (JLab) in 2009. JLab delivers, simultaneously, a nearly 100% duty factor polarized electrons into three experimental Halls (A, B, C). The data were collected over three months via projecting a 6.064 GeV longitudinally polarized beam, (83% polarization), on a 6 atm gaseous ^{4}He target. The Hall-B Large Acceptance Spectrometer (CLAS) basic design [22] was upgraded, during the CLAS-E1DVCS1 experimental run [11] in 2005, with a specially designed electromagnetic calorimeter, Inner calorimeter (IC). The IC has extended the photon detection acceptance of CLAS, which is originally from 15° to 45°, to polar angle reach as minimum as 4°. During the same experiment, a 5 Tesla solenoid was added around the target to shield the inner detectors from the low-energy Møller electrons.

At 6 GeV incident electron beam energy, the recoil ^{4}He nuclei, from the coherent DVCS channel, have an average momentum (per charge) around 125 MeV/c, while the CLAS spectrometer detects charged particles with a threshold of 250 MeV/c. In order to ensure the exclusivity of the our coherent DVCS channel, we built a small and light radial time projection chamber (RTPC) to detect recoiling nuclei down to energies of few MeVs. Figure 2 presents our cylindrical RTPC, which is 20 cm long and 15 cm diameter, surrounding the ^{4}He gaseous target and being inside the available space inside the solenoid , with a 3 cm radial drift length. The detector was specifically calibrated for ^{4}He nuclei using elastic scattering produced with a 1.2 GeV electron beam.

Identifying the coherent DVCS candidates is the first step of the data analysis. These events have one electron, one ^{4}He, and at least one photon in the final state. Electrons were identified by passing the fiducial cuts and having signals in all the sub-detectors of CLAS spectrometer (drift chambers, Cherenkov counters, the standard CLAS electromagnetic calorimeter, and scintillators). ^{4}He tracks were identified by passing all the geometrical, timing and quality cuts in the RTPC detector. The most energetic IC photon was considered as the DVCS photon candidate. Next, a $Q^2 > 1$ [GeV^2/c^2] cut is applied on the DVCS candidates in order to en-
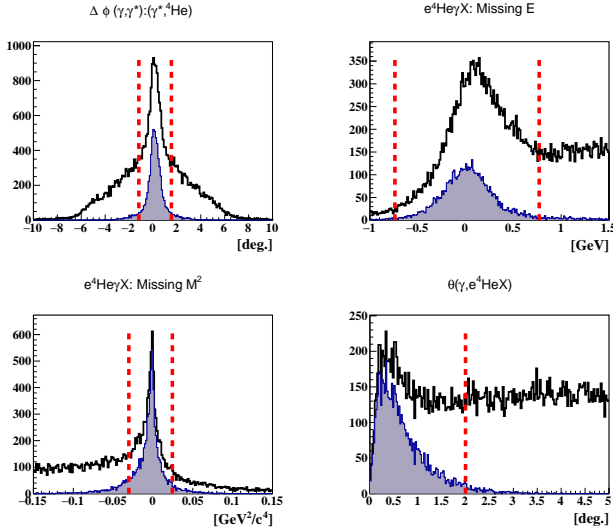
FIG. 3: Four of the seven coherent DVCS exclusivity cuts. The black distributions represent the coherent DVCS events candidate. The shaded distributions represent the events which passed all the exclusivity cuts except the quantity plotted. The vertical red lines represent 3σ cuts. The distributions from left to right and from top to bottoms are: $\Delta\phi$, missing energy and missing mass squared in $e'\ {}^4He'\ \gamma\ X$, and the cone angle (θ) between the measured and the calculated final state real photon.

FIG. 4: The Q^2 as a function of x_B (left) and the Q^2 as a function of $-t$ (right) for the identified coherent DVCS events after the exclusivity cuts.

sure that the interaction occurs at the partonic level and the applicability of the factorization in the DVCS hand-bag diagram. Once the three final state particles were identified with their 3-momentum vectors, the exclusivity of the coherent DVCS events were ensured by applied a set of 3σ exclusivity cuts. The exclusive cuts are: the co-planarity angle ($\Delta\phi$), missing energy, missing mass squared and missing transverse momentum in the $e'\ {}^4He'\ \gamma\ X$ final state configuration, the missing mass squared in the $e'\ {}^4He'\ X$ and $e'\ \gamma\ X$ configurations, and finally the cone angle (θ) between the measured real photon and the missing particle in the $e'\ {}^4He'\ X$ configuration. Figure 3 presents four of the applied exclusivity cuts.

After all the particle identification requirements on the individual particle of the coherent DVCS events and after all the exclusivity cuts, we ended up with about 3500 events. Figure 4 presents the (Q^2,x_B) and $(Q^2,-t)$ kinematic coverage of the collected DVCS events.

Even with all the previously presented exclusive cuts, the selected events are not all true DVCS events. We identified several background contributions to the coherent DVCS process, in particular accidental events and exclusive Deeply Virtual π^0 Production (DVπ^0P). The accidental events where the different particles come from different events are suppressed by the limited phase space allowed by the exclusivity cuts. We estimate the accidental events to represent 4.1% of our sample. This rel-
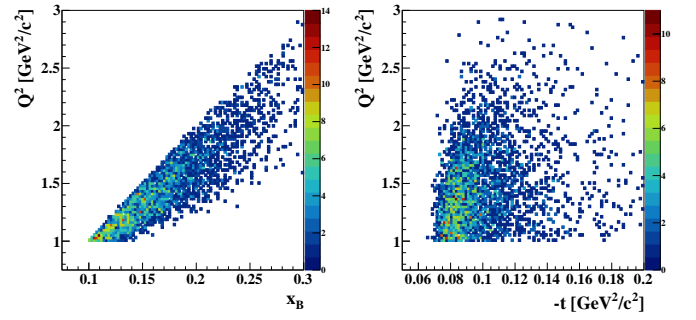
atively large number is due to the small cross section of the DVCS. We evaluated this contribution by selecting events passing all our cuts but with particles originating from different vertices. Regarding the DVπ^0P, which can easily be mistaken with DVCS when one of the two photons of the π^0 decay is produced at low energy in the laboratory frame. To estimate the importance of this background, we developed an event generator that we calibrated to match our measured experimental yield of exclusive π^0. We used this generator together with a GEANT3 simulation of our detection system to estimate the ratio of acceptance between DVπ^0P where the two photons are detected and those where only one photon is detected and would pass our DVCS selection cuts. This ratio obtained from simulation is then multiplied by the measured yield of DVπ^0P events, indicating a contamination of 2 to 4%. The study of systematics errors showed that the main contributions come from the choice of the DVCS exclusivity cuts (8%) and the large binning size (5.1%). However added quadratically, these errors sum up to 10% which remain for all bins well below the statistical errors.

The beam-spin asymmetry is our DVCS observable, which is measurable using a polarized lepton beam on an unpolarized target (U). It is convenient to use the beam-spin asymmetry as a DVCS observable because most of the experimental normalization and acceptance issues cancel out in the asymmetry ratio. It is defined in terms of the cross sections as:

$$A_{LU} = \frac{d^5\sigma^+ - d^5\sigma^-}{d^5\sigma^+ + d^5\sigma^-}. \tag{1}$$

where $d^5\sigma^+(d^5\sigma^-)$ is the DVCS differential cross section for a positive (negative) beam helicity. A_{LU} can be simplified in terms of the collected number of events in each beam-helicity state (N^+, N^-) as:

$$A_{LU} = \frac{1}{P_B}\frac{N^+ - N^-}{N^+ + N^-}. \tag{2}$$

where P_B is the beam polarization, and N^+ and N^- are

the number of events detected with positive and negative electron helicity, respectively. The statistical uncertainty of A_{LU} is

$$\sigma_{A_{LU}} = \frac{1}{P_B}\sqrt{\frac{1-(P_B A_{LU})^2}{N}} \tag{3}$$

where $N(N^+ + N^-)$ is the total number of measured events.

we extract the GPD H in a model independent way (figure 7). This is possible using the beam-spin asymmetry (A_{LU}) expression for spin-zero target at leading twist [23, 24]:

$$A_{LU}(\phi) =$$
$$\frac{\alpha_0(\phi)\,\Im m(\mathcal{H}_A)}{\alpha_1(\phi) + \alpha_2(\phi)\,\Re e(\mathcal{H}_A) + \alpha_3(\phi)\left(\Re e(\mathcal{H}_A)^2 + \Im m(\mathcal{H}_A)^2\right)} \tag{4}$$

where $\Im m(\mathcal{H}_A)$ and $\Re e(\mathcal{H}_A)$ are the imaginary and real parts of the CFF $\mathcal{H}_A$ associated to the GPD H_A. The α_i's are ϕ-dependent kinematical factors that depend on the nuclear form factor F_A and the independent variables Q^2, x_B and t. These factors are simplified as:

$$\alpha_0(\phi) = \frac{x_A(1+\epsilon^2)^2}{y}S_{++}(1)\sin(\phi) \tag{5}$$

$$\alpha_1(\phi) = c_0^{BH} + c_1^{BH}\cos(\phi) + c_2^{BH}\cos(2\phi) \tag{6}$$

$$\alpha_2(\phi) = \frac{x_A(1+\epsilon^2)^2}{y}(C_{++}(0) + C_{++}(1)cos(\phi)) \tag{7}$$

$$\alpha_3(\phi) = \frac{x_A^2 t(1+\epsilon^2)^2}{y}\mathcal{P}_1(\phi)\mathcal{P}_2(\phi)\cdot 2\frac{2-2y+y^2+\frac{\epsilon^2}{2}y^2}{1+\epsilon^2} \tag{8}$$

Where $S++(1)$, $C_{++}(0)$, and $C_{++}(1)$ are the Fourier harmonics in the leptonic tensor. Their explicit expressions can be found in .

We thank the staff of the Accelerator and Physics Divisions at Jefferson Lab for making this experiment possible.
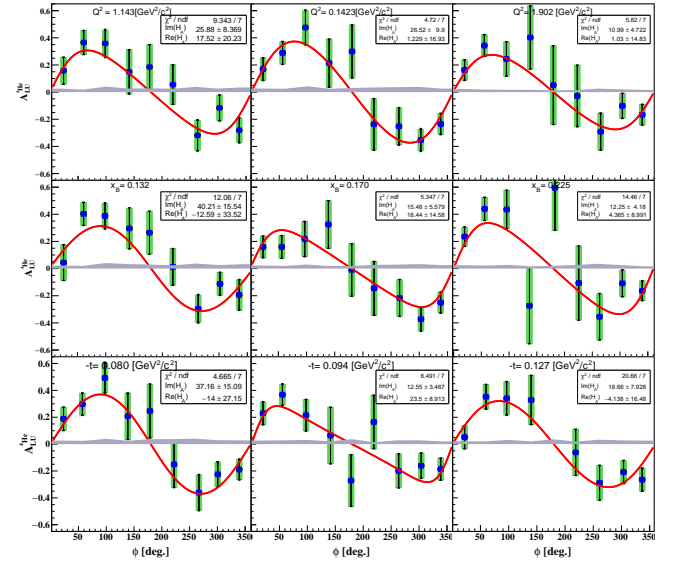

FIG. 5: The coherent A_{LU} as a function of ϕ in Q^2 (top panel), x_B (middle panel), and $-t$ (bottom panel) bins. The error bars represent the statistical and the systematic uncertainties added quadratically, shown on top in green are error bars representing only the statistical uncertainties. The brown bands represent the systematic uncertainties, including the normalisation systematic uncertainties. The red curves represent fits in the form of equation 4.
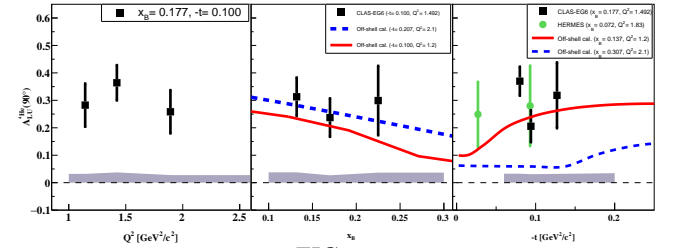

FIG. 6:

[1] M. Burkardt, Phys. Rev. D **62**, 071503 (2000) Erratum: [Phys. Rev. D **66**, 119903 (2002)]
[2] M. Diehl, Eur. Phys. J. C **25**, 223 (2002) Erratum: [Eur. Phys. J. C **31**, 277 (2003)]
[3] A. V. Belitsky and D. Mueller, Nucl. Phys. A **711**, 118 (2002)
[4] M. Burkardt, Phys. Rev. D **72**, 094020 (2005)
[5] S. Stepanyan *et al.* [CLAS Collaboration], Phys. Rev. Lett. **87**, 182002 (2001).
[6] A. Airapetian *et al.* [HERMES Collaboration], Phys. Rev. Lett. **87**, 182001 (2001); JHEP **1207**, 032 (2012); JHEP **1006**, 019 (2010); JHEP **0806**, 066 (2008); Phys. Lett. B **704**, 15 (2011); Phys. Rev. D **75**, 011103 (2007); JHEP **0911**, 083 (2009); Phys. Rev. C **81**, 035202 (2010); JHEP **1210**, 042 (2012).
[7] S. Chekanov *et al.* [ZEUS Collaboration], Phys. Lett. B **573**, 46 (2003).
[8] A. Aktas *et al.* [H1 Collaboration], Eur. Phys. J. C **44**, 1 (2005).
[9] S. Chen *et al.* [CLAS Collaboration], Phys. Rev. Lett. **97**, 072002 (2006).
[10] C. Muñoz Camacho *et al.* [Jefferson Lab Hall A Collaboration], Phys. Rev. Lett. **97**, 262002 (2006).
[11] F.X. Girod *et al.* [CLAS Collaboration], Phys. Rev. Lett. **100**, 162002 (2008).
[12] G. Gavalian *et al.* [CLAS Collaboration], Phys. Rev. C **80**, 035206 (2009).
[13] E. Seder *et al.* [CLAS Collaboration], Phys. Rev. Lett. **114**, 032001 (2015).
[14] S. Pisano *et al.* [CLAS Collaboration], Phys. Rev. D **91**, 052014 (2015).
[15] H. S. Jo *et al.* [CLAS Collaboration], Phys. Rev. Lett. **115**, no. 21, 212003 (2015)
[16] M. Mazouz *et al.* [Jefferson Lab Hall A Collaboration], Phys. Rev. Lett. **99**, 242501 (2007)
[17] A. Freund and J.C. Collins, Phys. Rev. D **59**, 074009 (1998)
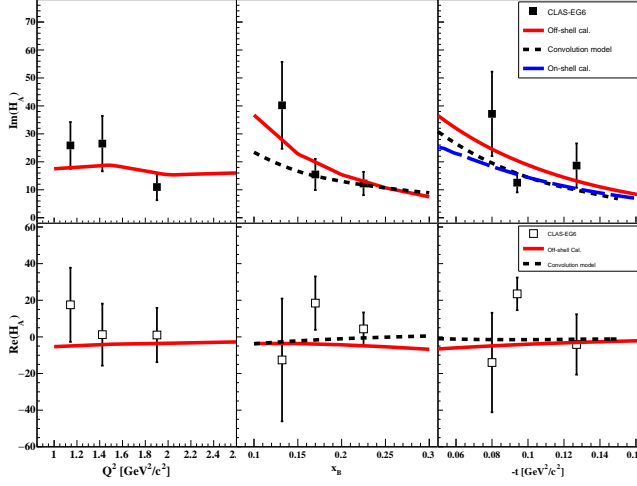[18] X.-D. Ji and J. Osborne, Phys. Rev. D **58**, 094018 (1998)

FIG. 7: The model-independent extraction of the imaginary (blue points) and real (red points) parts of the ^{4}He CFF $\mathcal{H}_A$, as functions of Q^2 (on the top right), x_B (on the top left), and t (on the bottom).

[19] A. V. Belitsky and A. V. Radyushkin, Phys. Rept. vol. 418 (2005)

[20] M. Guidal, H. Moutarde and M. Vanderhaeghen, Rept. Prog. Phys. **76**, 066202 (2013)

[21] J. Seely *et al.* Phys. Rev. Lett. **103**, 202301 (2009)

[22] B.A. Mecking *et al.*, Nucl. Inst. and Meth. A 503, 513 (2003)

[23] A. Kirchner and D. Mueller, Eur. Phys. J. C **32**, 347 (2003)

[24] A. V. Belitsky and D. Mueller, Phys. Rev. D **79**, 014017 (2009)

[25] F. Ellinghaus *et al.* [HERMES Collaboration], AIP Conf. Proc. **675**, 303 (2003)